iScience

CellPress
OPEN ACCESS

Article

A portable device for water-sloshing-based electricity generation based on charge separation and accumulation

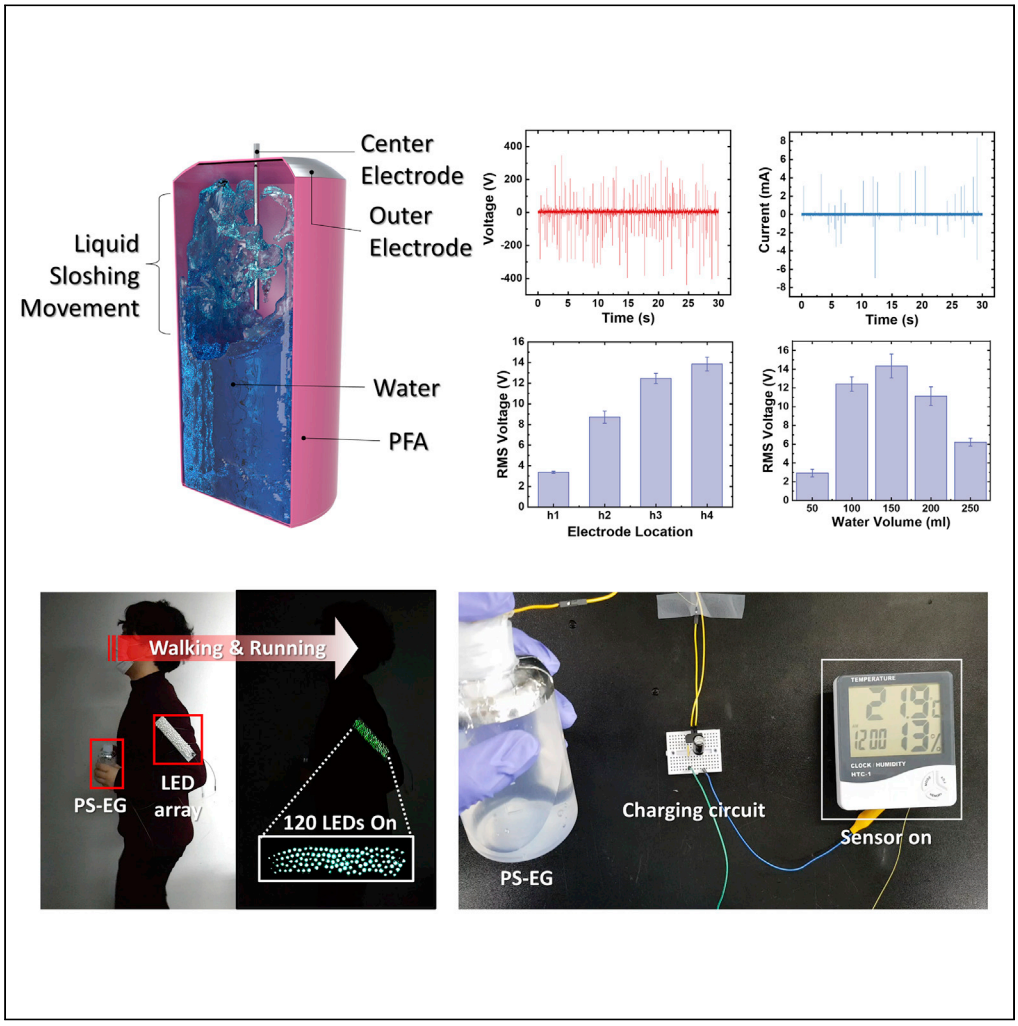

Jihoon Chung, Deokjae Heo, Kyunghwan Cha, Zong-Hong Lin, Jinkee Hong, Sangmin Lee

jkhong.yonsei@gmail.com (J.H.)
slee98@cau.ac.kr (S.L.)

Highlights

Portable electric generator using water sloshing motion is proposed

Quantitative analysis for optimized water generator design was done

Electrical power is generated through walking and running motion

Chung et al., iScience 24, 102442
May 21, 2021
https://doi.org/10.1016/j.isci.2021.102442

iScience

CellPress
OPEN ACCESS

Article

A portable device for water-sloshing-based electricity generation based on charge separation and accumulation

Jihoon Chung,[1,4] Deokjae Heo,[1,4] Kyunghwan Cha,[1,4] Zong-Hong Lin,[2] Jinkee Hong,[3,*] and Sangmin Lee[1,5,*]

SUMMARY

Hydropower generation is a well-known electricity generation technique that uses Faraday's law and hydraulic turbines. Recently, a triboelectrification-based electricity generation device, using water as the triboelectric material (W-TEG) was developed. In addition to the enhancement of the electrical output performance through the operation mechanism, the characteristics of the W-TEG must be examined at the design level to facilitate its portable application. Therefore, in this work, we developed a portable water-sloshing-based electricity generator (PS-EG) that can produce a high electric output and achieved its closed-loop circuit design and quantitative analysis for portable applications. The proposed PS-EG produced peak open-circuit voltage (V_{OC}) and closed-circuit current (I_{CC}) of up to 484 V and 4.1 mA, respectively, when subjected to vibrations of 2 Hz. The proposed PS-EG can be effectively used as an auxiliary power source for small electronics and sensors.

INTRODUCTION

Water, which covers 70% of the Earth's surface and serves as a promising alternative energy source, can be used in electric power generation. Hydropower generation in which the dynamic energy of falling or flowing water is converted to electricity is a widely used electricity generation technique that applies Faraday's law to hydraulic turbines. With the advancement of the Internet of things, which relies on small/thin electronics or self-powered sensors, researchers are attempting to ensure a balance between the portability and electrical output of energy harvesters. Furthermore, various energy harvesters that use the electrokinetic effect (Duffin and Saykally, 2008; Koranlou et al., 2019) or triboelectrification (Kim et al., 2018a, 2019; Zhu et al., 2012; Fan et al., 2012; He et al., 2017) techniques have been developed to generate the electric power necessary to power small electronics. Among such devices, triboelectrification-based electricity generators, which are made of lightweight materials and can produce a high electrical output, have demonstrated potential to function as auxiliary power sources of small electronic devices or self-powered sensors (Wang, 2017; Chung et al., 2019; Hwang et al., 2019; Meng et al., 2013; Kim et al., 2019). Existing works on water-based triboelectric generators (W-TEGs) involved the use of water hydraulics to induce solid-solid contact (Zhang et al., 2020b; Kim et al., 2018b; Xu et al., 2019) and the electrical aspects of water Lee et al. (2016), Chung et al. (2018), Lin et al. (2014), Jang et al. (2020), Cho et al. (2019) (Helseth, 2020; Helseth and Guo, 2015; Helseth and Guo, 2016) to exploit liquid-solid contact. However, owing to the mechanism of triboelectrification, solid-solid contact generators are highly vulnerable to wear failure and humidity (Mule et al., 2019; Nguyen and Yang, 2013). Consequently, it is desirable to develop W-TEGs with liquid-solid contact to ensure an extended lifespan and constant electrical output in humid environments.

The key challenges for the practical implementation of liquid-solid contact W-TEGs in portable applications are to enhance the electrical output performance and realize a portable design. Recently, the electrical output performance of W-TEGs was considerably improved from the nanowatt-to-microwatt scale by inducing direct contact between the water and a conductive material (Xu et al., 2020; Zhang et al., 2020a; Chung et al., 2021). Although the development of a working mechanism to realize a high electrical output is in progress, the characteristics of W-TEGs must be examined at the design level to ensure their suitability for portable applications. In this regard, W-TEGs with a closed-loop circuit are preferable, as no additional circuit for the electrical ground is required, and the device is more efficient than single-electrode

[1]School of Mechanical Engineering, Chung-ang University, 84, Heukseok-ro, Dongjak-gu, Seoul, Republic of Korea

[2]Institute of Biomedical Engineering and Department of Power Mechanical Engineering, National Tsing Hua University, 101, Section 2, Kuang-Fu Road, Hsinchu 30013, Taiwan

[3]Department of Chemical & Biomolecular Engineering, College of Engineering, Yonsei University, 50 Yonsei-ro, Seodaemun-gu, Seoul 03722, Republic of Korea

[4]These authors contributed equally

[5]Lead contact

*Correspondence: jkhong.yonsei@gmail.com (J.H.), slee98@cau.ac.kr (S.L.)

https://doi.org/10.1016/j.isci.2021.102442

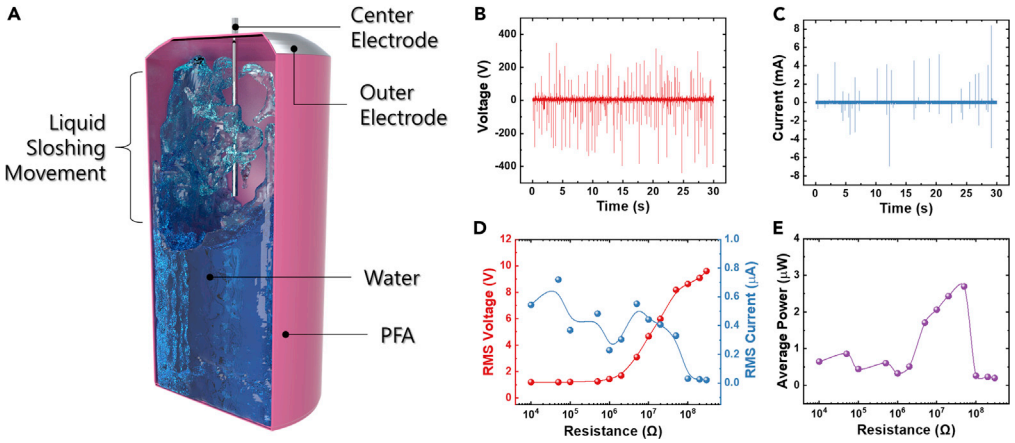

Figure 1. Schematic and electrical performance of portable water-sloshing-based electric power generator (PS-EG)

(A) Schematic illustration of PS-EG.

(B–E) (B) V_{OC} and (C) I_{CC} performance of PS-EG. Root-mean-square (RMS) (D) voltage, current, and (E) power performance of PS-EG.

generators (Meng and Chen, 2020). In addition, because a high electrical output is generated only when water in motion contacts the conductive material, the relationship between the water motion and electrical characteristics must be quantitatively analyzed. Therefore, it is desirable to realize an extensive design and analysis of liquid-solid contact W-TEGs.

To this end, in this work, through a closed-loop circuit design and quantitative analyses, we developed a water-sloshing-based electricity generator (PS-EG) that can produce a high electric output. The PS-EG is composed of a dielectric container (perfluoroalkoxy alkane [PFA]) containing water, a central electrode, and an outer electrode. When mechanical input is applied to the container, charge separation and accumulation occur owing to the self-ionization of water under the electric field induced by the negative surface charge of the PFA container. The dynamic motion of water, which induces the charge separation and accumulation, can be categorized as wall impact, wave motion, or water-droplet-related motion. Considering these mechanical movements, quantitative analyses were performed on the optimized device design, based on the location of the outer electrode and amount of water, examining the peak and root-mean-square (RMS) output. The proposed PS-EG could power 120 light emitting diodes (LEDs) continuously during walking or running activities and demonstrated promising potential for implementation in everyday applications.

RESULT AND DISCUSSION

The PS-EG consists of four basic components: a dielectric container, two electrodes, and water (Figure 1A). PFA was used as the dielectric material because the associated negative surface charges can induce a strong electric field owing to its high electron affinity. The central electrode was electrically connected to the outer electrode in a closed-loop circuit. In general, when a container vibrates vertically, water inside the container no longer remains stationary. The movement of water inside a container is often termed as "sloshing motion" (Hashimoto and Sudo, 1988; Ibrahim et al., 2001). During this movement, charge separation and accumulation occur in water owing to the self-ionization of water. In particular, water naturally undergoes self-ionization and produces negative (hydroxide ion [OH^-]) and positive charges (hydrogen ion [H^+]/hydronium ion [H_3O^+]) (Pitzer, 1982). Owing to the mechanical movement of the water in the PFA container, the electric field of the container leads to the separation and accumulation of the charges. When water with the accumulated charge contacts the central electrode, electricity is generated as per the water behavior. When a vertical excitation of 6 Hz is continuously applied by a vibration tester to the container, the water behavior, although irregular and complex, can be divided into three types (Chung et al., 2021): wall impact, wave motion, and water-droplet-related motion. First, when water impacts a wall of the container and moves along the negative wall surface, net positive charges of water are induced, forming an electrical double layer, which consists of a stern layer and diffuse layer. The stern layer is an immobile region in which the positive ions of water adhere to the negative surface of the PFA. Even if water

continues to slide against the PFA surface, the stern layer remains immobile. In the mobile diffuse layer, which is present next to the stern layer, positive or negative ions can move freely, and the positive ions are attracted by the strong negative surface charges of the PFA. Until the Debye length, at which the negative surface charges of the PFA are fully screened by the ions and water molecules, is reached, water exhibits a net positive charge (Figure S1). Therefore, as water impacts and propagates on the wall surface of the PFA, the positive charges of water are continuously induced and accumulated. When these accumulated positive charges contact the central electrode, a distinctively high electrical peak is generated. Second, when water in the middle of the container oscillates longitudinally in a wave motion, negative charges are accumulated owing to the high positive charge concentration of water near the PFA wall surface. Simultaneously, positive charges are induced at the central electrode, owing to the negative surface charge of the PFA. When water at the center of the container rises and contacts the central electrode, a negative peak output is generated (Chung et al., 2021). Third, water droplets may be separated from the bulk water surface during the wall impact and wave motions. These water droplet fragments exhibit either a positive or negative charge according to the Poisson model (Wiederschein et al., 2015). Thus, when a water droplet contacts the electrodes, positive and negative peak outputs are produced. Notably, the electrical output from the wall impact and water-droplet-related motion is higher than that corresponding to the wave motion. Moreover, because the water movement in the PS-EG involved substantial wall impacts and droplets contacting the central electrode, the high electrical output of the PS-EG can be attributed primarily to these behaviors.

Figures 1B and 1C show the peak open-circuit voltage (V_{OC}) and closed-circuit current (I_{CC}) at a vertical input frequency of 6 Hz, respectively. The maximum V_{OC} and I_{CC} were 440 V and 8.4 mA, respectively. Total amount of transferred charges between the electrodes also can be calculated by integrating peak current in Figure 1C. The total charges transferred between the electrodes for 30 s is 0.39 mC. Moreover, the voltage and current pertaining to various external load resistances were measured and converted into RMS voltage (V_{RMS}) and current (I_{RMS}) values, as follows.

$$V_{RMS} = \sqrt{\frac{\int V(t)^2 dt}{T}},\ I_{RMS} = \sqrt{\frac{\int I(t)^2 dt}{T}}$$

where $V(t)$, $I(t)$, and T denote the measured peak voltage, peak current output, and measurement period, respectively.

In general, the RMS value is a quantitative indicator and does not reflect the peak output value, and the waveform generated by the PS-EG is an extremely sharp peak. Therefore, it is necessary to examine the RMS output to evaluate the suitability of the device for use as an auxiliary power source for small electronics. The converted V_{RMS} and I_{RMS} values of the PS-EG at various external load resistances are shown in Figure 1D. With the increase in the external load resistance, the RMS voltage and current increase and decrease, respectively. Figure 1E shows the average power plot obtained by multiplying the V_{RMS} and I_{RMS} values at each external load resistance. It can be noted that the PS-EG generates a maximum average power of 2.69 μW at an external load resistance of 50 MΩ.

Figure 2A shows the electrical output of the PS-EG, measured at different positions of the outer electrode (h_1–h_4). In general, for the PS-EG to be used in portable applications, a dual electrode configuration must be used to eliminate the requirement of an electrical ground; moreover, a single electrode is usually less efficient than a dual electrode (Meng and Chen, 2020). As the PS-EG is cylindrical and exhibits vertical motion, the electrode on the outer surface of the dielectric container can be adjusted. When vertical excitation of 6 Hz is applied to the PS-EG through a vibration tester, water inside the container exhibits three types of dynamic behaviors and contacts each electrode.

Figures 2B and 2C show the average peak voltage and V_{RMS} output of the PS-EG at different outer electrode locations (h_1–h_4), and Figure S3 shows the voltage versus time plots corresponding to these locations. The outer electrode locations are equally spaced; specifically, h_1 to h_4 are located from the bottom to the top of the container at equal intervals. The plots indicate that both the average peak voltage and V_{RMS} exhibit similar tendencies. When the outer electrode is located at h_1, the lowest average peak voltage output and RMS voltage output are 61 V and 3.3 V, respectively. The average peak voltage and V_{RMS} increase as the position of the outer electrode shifts to the top, that is, from h_2 to h_4. The highest average peak voltage and RMS voltage (204 V and 13.8 V, respectively) occur when the outer electrode is located at h_4.

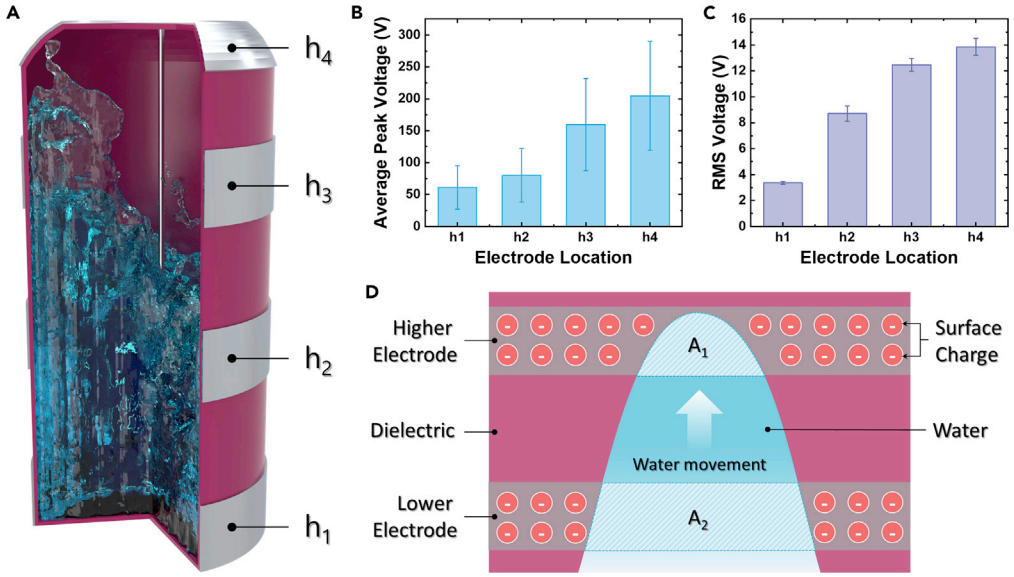

Figure 2. Electrical performance of the PS-EG, for different locations of the electrode

(A) Schematic illustration of different locations of electrode on PS-EG.

(B and C) (B) Average peak voltage, and (C) RMS voltage depending on different locations of electrode.

(D) Illustration on water movement depending on different location of electrode.

As mentioned previously, the main behaviors of water that produce a high electrical output are the wall impact and water-droplet-related motion. Considering the amount of water in motion, wall impact is the water movement that most notably affects the electrical output of the PS-EG. When the PFA container is excited vertically, water starts to slosh inside the container, and wall impact motion occurs. When water propagates to the top of the PFA container, the water mass appears triangular owing to the influence of gravity (Figures 2D and S4). Owing to this phenomenon, when two electrodes are located at high and low positions, the contact area (A_1 and A_2, respectively) between the PFA and water is larger on the electrode that is placed lower ($A_1 < A_2$). In the contact area, the surface charge of the PFA is screened by the ions and molecules of water, owing to which the electrode behind the PFA (outer electrode) exhibits a lower induced charge. Because the measured output of the PS-EG is mainly based on the electrical potential difference between the two electrodes when water contacts the central electrode, the generated output is expected to decrease when a larger amount of surface charge of the PFA is screened by water.

Furthermore, Figure S5A shows the average peak voltage and V_{RMS} output of the PS-EG for different center electrode length of 1, 2, 3, 4, and 5 cm. The voltage versus time plot corresponding to these lengths is shown in Figure S5B. Center electrode length of more than 5 cm, which reaches water surface of 150 mL, is not considered. When the center electrode is 1 cm, the lowest average peak voltage of 93.6 V and RMS voltage of 6.1 V are generated. The average peak voltage and V_{RMS} increase as the length of center electrode increase from 1 cm to 5 cm. The highest average peak voltage of 177.5 V and RMS voltage of 13.2 V are produced when center electrode is 5 cm. It is because that water with accumulated charges is more likely to contact the center electrode as the center electrode length increases. Figure S6A represents the average peak voltage and RMS voltage output of the PS-EG at PFA thickness of 1T (0.55 mm) and 2T (0.1 mm). Figure S6B shows the voltage versus time plot corresponding to these thicknesses. When the PFA thickness is 1T, average peak voltage of 125.1 V and RMS voltage of 10.2 V are generated. The PS-EG with thickness of 2T also produced average peak voltage of 144.8 V and RMS voltage of 10.7 V, comparable with those for 1T. As a result, it is expected that PFA thickness does not significantly affect electrical performance of the PS-EG.

Figure 3A shows a schematic of the PS-EG pertaining to different amounts of water inside the PFA container (water volume of 50, 100, 150, 200, and 250 mL). When a vertical vibration is applied to the PS-EG, water inside the container exhibits different mechanical movements depending on the water volume. Figures 3B and 3C show the average peak voltage and V_{RMS} output of the PS-EG for different values of the water volume (50–250 mL). The V_{OC} versus time plot for each value of the water volume is shown in Figure S7.

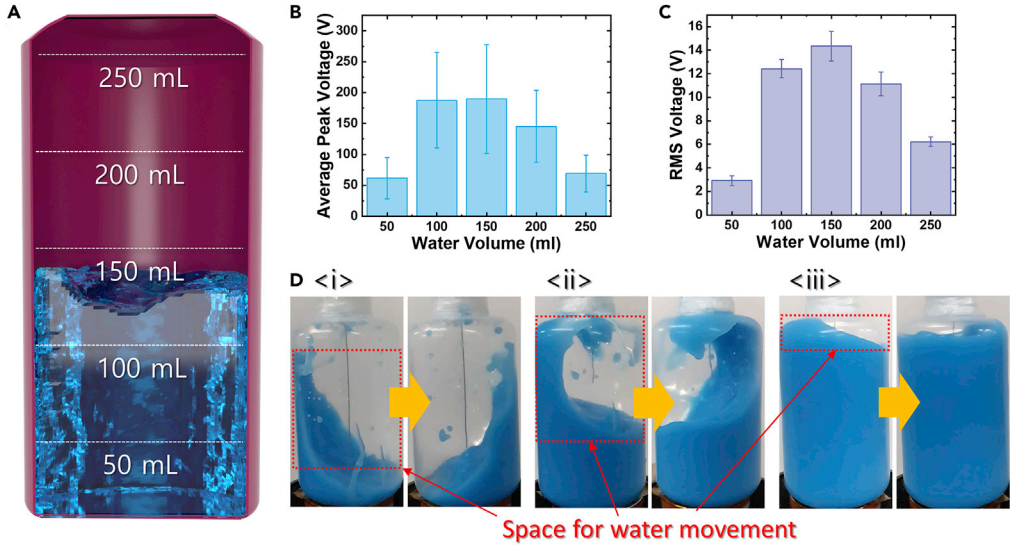

Figure 3. Electrical performance of the PS-EG for different values of the water volume

(A) Schematic of the water level pertaining to the volume of water inside the container.

(B and C) (B) Average peak voltage and (C) RMS voltage of the PS-EG for different values of the water volume.

(D) Photograph of water sloshing inside the PFA container for a water volume of (i) 50 mL, (ii) 150 mL, (iii) 250 mL.

When the volume of water is 150 mL, which is the volume corresponding to the midline of the PFA container, the highest peak voltage of 189 V and V_{RMS} of 14 V are generated. The volume of 50 mL corresponds to the smallest peak voltage of 61 V and V_{RMS} of 2.9 V. The peak voltage and V_{RMS} corresponding to the volume of 250 mL are also small, 69 V and 6.2 V, respectively, comparable with those for the volume of 50 mL.

In general, water with accumulated charge generates electricity when it contacts the central electrode; therefore, the main factors influencing the charge accumulation inside water are the PFA surface and disruption of the water surface (Wiederschein et al., 2015; Shewchuk and Iribarne, 1971; Lenard, 1892). In other words, for water to have a higher accumulated charge, water must contact and propagate more on the PFA surface and must have sufficient space to exhibit mechanical movement. Specifically, the PS-EG can produce a higher output when both these factors are satisfied. Figure 3D shows high-speed camera photographs of the water behavior for volumes of 50, 150, and 250 mL (Videos S1, S2, and S3), which correspond to the volume of water that is below, exactly at, and above the midline of the PFA container, respectively. As shown in Figure 3D-i, although a volume of 50 mL (below midline of PFA container) means that water has sufficient free space to move, owing to the limited volume, the contact area between the PFA and water is smaller than that for the water volume of 150 mL. When the water volume is 150 mL, water has sufficient space to move, and the contact area is larger than that when the volume is 50 mL, which increases the charge separation and charge accumulation, thereby leading to the generation of a high electrical output (Figure 3D-ii). As shown in Figure 3D-iii, when the water volume is 250 mL, (above the midline of the PFA container), water does not have sufficient space to move or contact the PFA. These results indicate that the largest electrical output is generated when the water level is near the midline of the dielectric container.

The proposed PS-EG can be applied directly in everyday applications. Figure 4A shows a schematic of the PS-EG as a self-powered water bottle with a straw, consisting of a PFA bottle containing water, an outer electrode, and electrode-coated straw as the central electrode. When the water bottle is swung owing to hand or body motion, water inside the bottle exhibits sloshing movement and contacts the central electrode. During daily walking or running activities, the PS-EG can power 120 LEDs attached on the forearm, through a full-wave bridge rectifier, as shown in Figure 4B. The details of the rectification circuit are shown in Figure S8. Videos S4 and S5 show that the 120 LEDs are continuously lit when the device is shaken by the hand and during running motion in which the PS-EG is subjected to vibrations with a frequency of 2 Hz. Figures 4C and 4D show the detailed peak open-circuit voltage (V_{OC}) and peak closed-circuit current (I_{CC}) plots under a manual vibration input frequency of 2 Hz, respectively. A maximum peak V_{OC} and peak I_{CC}

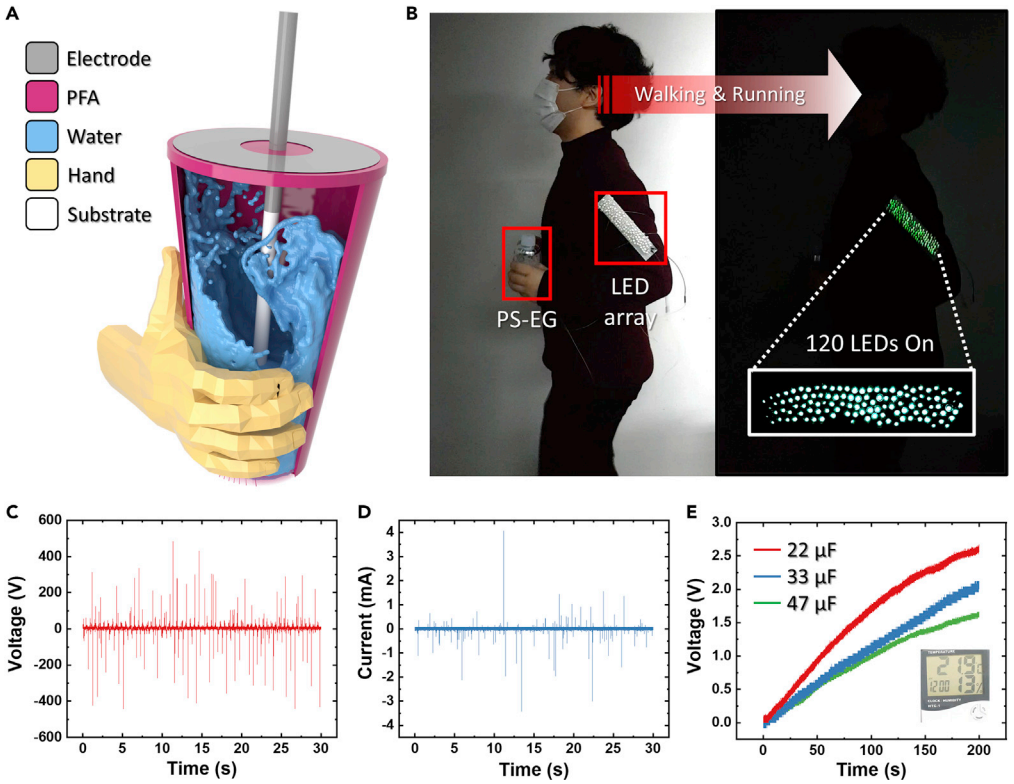

Figure 4. Schematic and electrical performance of commercial cup-type PS-EG, for different values of the water volume

(A) Schematic of the PS-EG designed as a commercial cup.

(B) PS-EG powering 120 LEDs during walking and running activities.

(C and D) (C) V_{OC} and (D) I_{CC} output when vibration with a frequency of 2 Hz is applied to the PS-EG.

(E) PS-EG charging a commercial capacitor.

of 484 V and 4.1 mA are produced, respectively. Moreover, the PS-EG can charge energy storage units, such as capacitors. To demonstrate the charging capability, a commercial capacitor with different load capacitances is charged using the PS-EG. Figure 4E shows the charging plot of the PS-EG for 22, 33, and 47 μF capacitances for 200 s, during manual shaking with a frequency of 2 Hz. Figure S9 presents the details of the charging circuit in which the capacitor is connected to a full-wave bridge rectifier. Furthermore, the PS-EG can charge 330-μF capacitor and power portable digital clock temperature-humidity meter by charging a capacitor. Figure S10 shows detailed charging circuit and the photograph powering portable digital clock temperature-humidity meter. Video S6 shows that the PS-EG can power digital clock temperature-humidity meter after 40-min charging. The proposed PS-EG can be effectively integrated in various applications in everyday life. For example, the water-bottle-type PS-EG can serve as a portable self-powered safety lamp as well as an auxiliary power source for small electronics such as a safety tracking device while an individual is climbing a mountain or walking and running at night. As shown in Figure S11, even after 24 h of operation, the PS-EG has shown consistent output.

Conclusions

We developed a PS-EG that can generate a high electrical output through water movement. The device has a simple design involving a dielectric container containing water and two electrodes. When water sloshes inside the dielectric container, the water ions are separated, leading to accumulated charge. As the water with the accumulated charge contacts the central electrode, a distinctively high electrical output is generated. The electrical output of the PS-EG corresponding to different electrode positions and water volumes inside the container was measured, and it was noted that the highest output was generated when the electrode was located at the top of the dielectric container, with the water volume corresponding to the midline of the container. The proposed PS-EG produced a peak V_{OC} and I_{CC} of up to 484 V and 4.1 mA, respectively,

when subjected to vibrations of 2 Hz. The proposed PS-EG can be used as an auxiliary power source for small electronics and sensors.

Limitations of the study

The PS-EG device developed in this study can be used as effective mechanical energy harvester. However, the electrical output of the device can be further improved when solid material with greater surface charge compared with PFA is used. In addition, the PS-EG developed in this article mainly focus on using water as liquid material, but the concept of PS-EG has potential be used in other liquids as well. In the future studies can explore the influence of using different solid/liquid materials to increase the electrical output using current generator design.

Resource availability

Lead contact

Further information and requests for resources and reagents should be directed to and will be fulfilled by the lead contact Sangmin Lee (slee98@cau.ac.kr).

Material availability

Materials used in the study are commercially available.

Data and code availability

This study did not generate computer code. All data and analytical methods are available in the main text or in supplemental information section.

METHODS

All methods can be found in the accompanying transparent methods supplemental file.

SUPPLEMENTAL INFORMATION

Supplemental information can be found online at https://doi.org/10.1016/j.isci.2021.102442.

ACKNOWLEDGMENTS

This work was supported by the National Research Foundation of Korea (NRF) grant funded by the Korean government (MSIT) (No. 2020R1A2C1010829), and Nano·Material Technology Development Program through the National Research Foundation of Korea (NRF-2016M3A7B4910532)

AUTHOR CONTRIBUTIONS

J.C. and D.H. designed experiments and wrote the manuscript. J.C., D.H. and K.C. performed experiments. J.C., D.H., and K.C. analyzed the data. Z.L., J.H. and S.L provided expertise and feedback.

DECLARATION OF INTERESTS

The authors declare no competing interests.

Received: October 29, 2020
Revised: January 20, 2021
Accepted: April 13, 2021
Published: May 21, 2021

REFERENCES

Cho, H., Chung, J., Shin, G., Sim, J.Y., Kim, D.S., Lee, S., and Hwang, W. (2019). Toward sustainable output generation of liquid-solid contact triboelectric nanogenerators: the role of hierarchical structures. Nano Energy *56*, 56–64.

Chung, J., Heo, D., Kim, B., and Lee, S. (2018). Superhydrophobic water-solid contact triboelectric generator by simple spray-on fabrication method. Micromachines *9*, 593.

Chung, J., Heo, D., Shin, G., Choi, D., Choi, K., Kim, D., and Lee, S. (2019). Ion-enhanced field emission triboelectric nanogenerator. Adv. Energy Mater. *9*, 1901731.

Chung, J., Heo, D., Shin, G., Chung, S., Hong, J., and Lee, S. (2021). Water behavior based electric generation via charge separation. Nano Energy *82*, 105687.

Duffin, A.M., and Saykally, R.J. (2008). Electrokinetic power generation from liquid water microjets. J. Phys. Chem. C *112*, 17018–17022.

Fan, F.R., Tian, Z.Q., and Wang, Z.L. (2012). Flexible triboelectric generator! Nano Energy *1*, 328–334.

Hashimoto, H., and Sudo, S. (1988). Violent liquid sloshing in vertically excited cylindrical containers. Exp. Therm. Fluid Sci. *1*, 159–169.

He, C., Zhu, W.J., Chen, B.D., Xu, L., Jiang, T., Han, C.B., Gu, G.Q., Li, D.C., and Wang, Z.L. (2017). Smart floor with integrated triboelectric nanogenerator as energy harvester and motion sensor. Acs Appl. Mater. Interfaces *9*, 26126–26133.

Helseth, L. (2020). A water droplet-powered sensor based on charge transfer to a flow-through front surface electrode. Nano Energy *73*, 104809.

Helseth, L., and Guo, X. (2015). Contact electrification and energy harvesting using periodically contacted and squeezed water droplets. Langmuir *31*, 3269–3276.

Helseth, L., and Guo, X. (2016). Fluorinated ethylene propylene thin film for water droplet energy harvesting. Renew. Energy *99*, 845–851.

Hwang, H.J., Kim, J.S., Kim, W., Park, H., Bhatia, D., Jee, E., Chung, Y.S., Kim, D.H., and Choi, D. (2019). An ultra-mechanosensitive visco-poroelastic polymer ion pump for continuous self-powering kinematic triboelectric nanogenerators. Adv. Energy Mater. *9*, 1803786.

Ibrahim, R.A., Pilipchuk, V., and Ikeda, T. (2001). Recent Advances in Liquid Sloshing Dynamics. Appl. Mech. Rev. Mar. *54*, 133–199.

Jang, S., La, M., Cho, S., Yun, Y., Choi, J.H., Ra, Y., Park, S.J., and Choi, D. (2020). Monocharged electret based liquid-solid interacting triboelectric nanogenerator for its boosted electrical output performance. Nano Energy *70*, 104541.

Kim, B., Chung, J., Moon, H., Kim, D., and Lee, S. (2018a). Elastic spiral triboelectric nanogenerator as a self-charging case for portable electronics. Nano Energy *50*, 133–139.

Kim, D.Y., Kim, H.S., Kong, D.S., Choi, M., Kim, H.B., Lee, J.H., Murillo, G., Lee, M., Kim, S.S., and Jung, J.H. (2018b). Floating buoy-based triboelectric nanogenerator for an effective vibrational energy harvesting from irregular and random water waves in wild sea. Nano Energy *45*, 247–254.

Kim, W., Bhatia, D., Hwang, H.J., Choi, K., and Choi, D. (2019). Double impact triboelectric nanogenerators for harvesting broadband vibrations from vehicles. Funct. Compos. Struct. *1*, 035003.

Koranlou, A., Ashrafizadeh, S.N., and Sadeghi, A. (2019). Enhanced electrokinetic energy harvesting from soft nanochannels by the inclusion of ionic size. J. Phys. D Appl. Phys. *52*, 155502.

Lee, S., Chung, J., Kim, D.Y., Jung, J.Y., Lee, S.H., and Lee, S. (2016). Cylindrical water triboelectric nanogenerator via controlling geometrical shape of anodized aluminum for enhanced electrostatic induction. Acs Appl. Mater. Interfaces *8*, 25014–25018.

Lenard, P. (1892). Ueber die Electricität der Wasserfälle. Annalen der Physik *282*, 584–636.

Lin, Z.H., Cheng, G., Lee, S., Pradel, K.C., and Wang, Z.L. (2014). Harvesting water drop energy by a sequential contact-electrification and electrostatic-induction process. Adv. Mater. *26*, 4690–4696.

Meng, Z., and Chen, L. (2020). Theoretical maximum efficiency and higher power output in triboelectric nanogenerators. Energy Rep. *6*, 2463–2475.

Meng, B., Tang, W., Zhang, X.S., Han, M.D., Liu, W., and Zhang, H.X. (2013). Self-powered flexible printed circuit board with integrated triboelectric generator. Nano Energy *2*, 1101–1106.

Mule, A.R., Dudem, B., Graham, S.A., and Yu, J.S. (2019). Humidity sustained wearable pouch-type triboelectric nanogenerator for harvesting mechanical energy from human activities. Adv. Funct. Mater. *29*, 1807779.

Nguyen, V., and Yang, R. (2013). Effect of humidity and pressure on the triboelectric nanogenerator. Nano Energy *2*, 604–608.

Pitzer, K.S. (1982). Self-ionization of water at high temperature and the thermodynamic properties of the ions. J. Phys. Chem. *86*, 4704–4708.

Shewchuk, S., and Iribarne, J. (1971). Charge separation during splashing of large drops on ice. Q. J. R. Meteorol. Soc. *97*, 272–282.

Wang, Z.L. (2017). On Maxwell's displacement current for energy and sensors: the origin of nanogenerators. Mater. Today *20*, 74–82.

Wiederschein, F., Vøhringer-Martinez, E., Beinsen, A., Postberg, F., Schmidt, J., Srama, R., Stolz, F., Grubmþller, H., and Abel, B. (2015). Charge separation and isolation in strong water droplet impacts. Phys. Chem. Chem. Phys. *17*, 6858–6864.

Xu, M., Zhao, T., Wang, C., Zhang, S.L., Li, Z., Pan, X., and Wang, Z.L. (2019). High power density tower-like triboelectric nanogenerator for harvesting arbitrary directional water wave energy. ACS Nano *13*, 1932–1939.

Xu, W., Zheng, H., Liu, Y., Zhou, X., Zhang, C., Song, Y., Deng, X., Leung, M., Yang, Z., and Xu, R.X. (2020). A droplet-based electricity generator with high instantaneous power density. Nature *578*, 392–396.

Zhang, N., Gu, H., Zheng, H., Ye, S., Kang, L., Huang, C., Lu, K., Xu, W., Miao, Q., and Wang, Z. (2020a). Boosting the output performance of volume effect electricity generator (VEEG) with water column. Nano Energy *73*, 104748.

Zhang, N., Qin, C., Feng, T., Li, J., Yang, Z., Sun, X., Liang, E., Mao, Y., and Wang, X. (2020b). Non-contact cylindrical rotating triboelectric nanogenerator for harvesting kinetic energy from hydraulics. Nano Res. *13*, 1–5.

Zhu, G., Pan, C.F., Guo, W.X., Chen, C.Y., Zhou, Y.S., Yu, R.M., and Wang, Z.L. (2012). Triboelectric-generator-driven pulse electrodeposition for micropatterning. Nano Lett. *12*, 4960–4965.

iScience, Volume *24*

Supplemental information

A portable device for water-sloshing-based electricity generation based on charge separation and accumulation

Jihoon Chung, Deokjae Heo, Kyunghwan Cha, Zong-Hong Lin, Jinkee Hong, and Sangmin Lee

Supplementary Figures

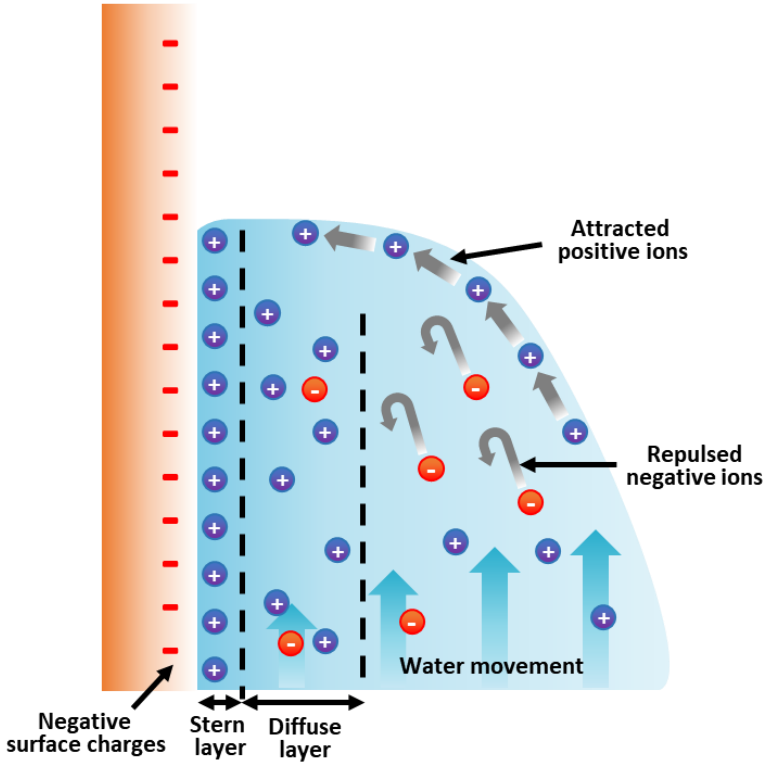

Figure S1. Schematic illustration of ion movement due to external electric field. Related to Figure 1.

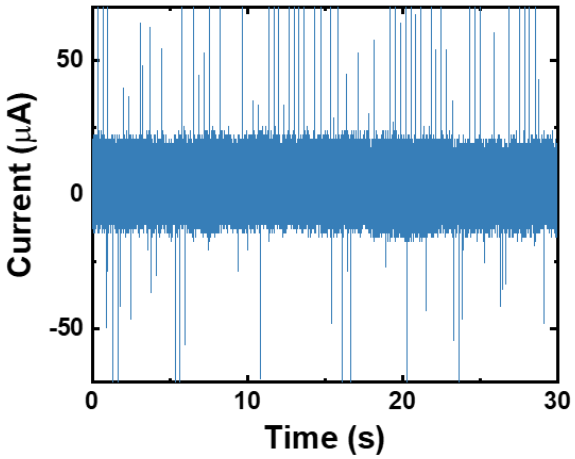

Figure S2. Magnified closed-circuit current output plot. Related to Figure 1.

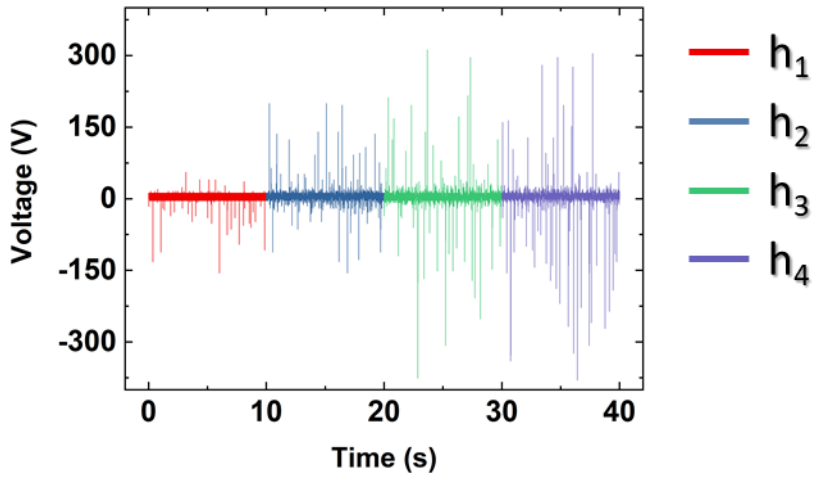

Figure S3. Open-circuit voltage output depending on the position of electrode. Related to Figure 2.

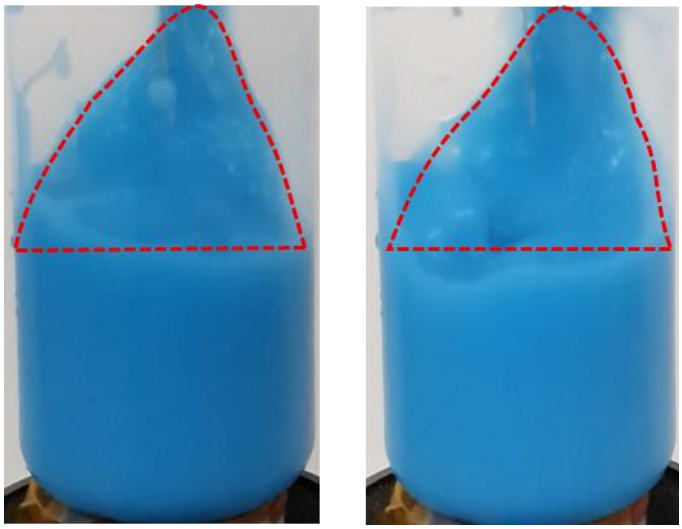

Figure S4. Moving water forming a triangular shape due to input force. Related to Figure 2.

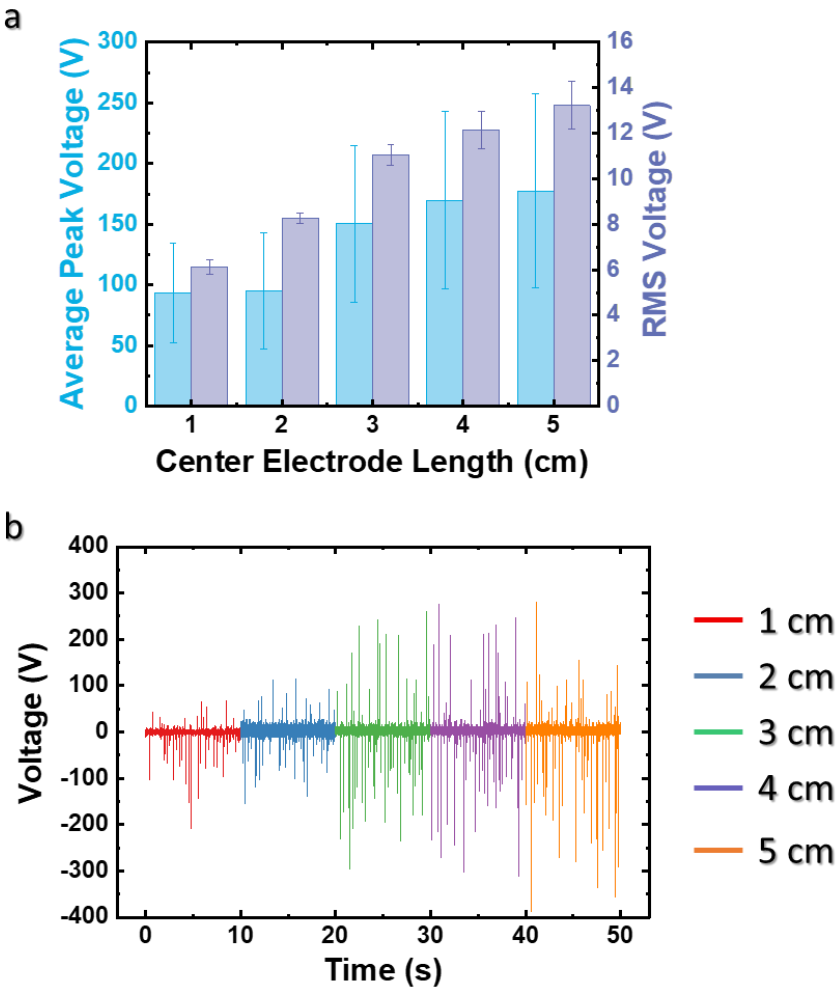

Figure S5. (a) Average peak voltage and RMS voltage output and (b) Open-circuit voltage plot depending on center electrode length. Related to Figure 2.

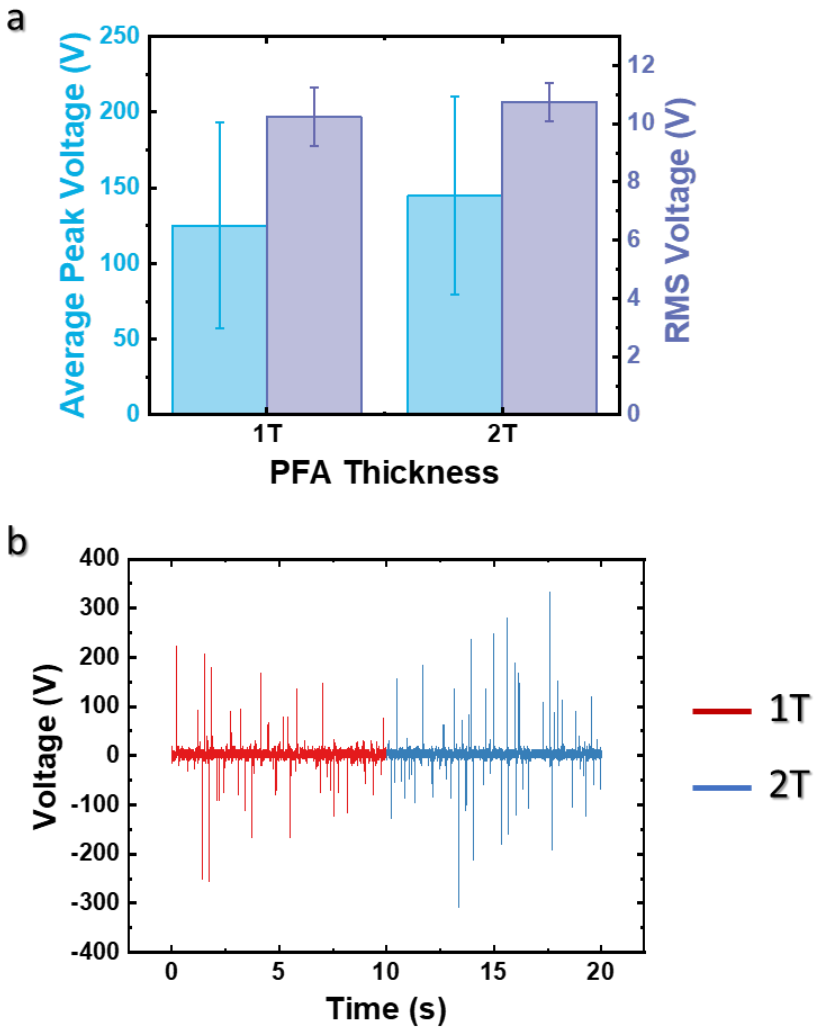

Figure S6. (a) Average peak voltage and RMS voltage output and (b) Open-circuit voltage plot at PFA thickness of 1T and 2T. Related to Figure 2.

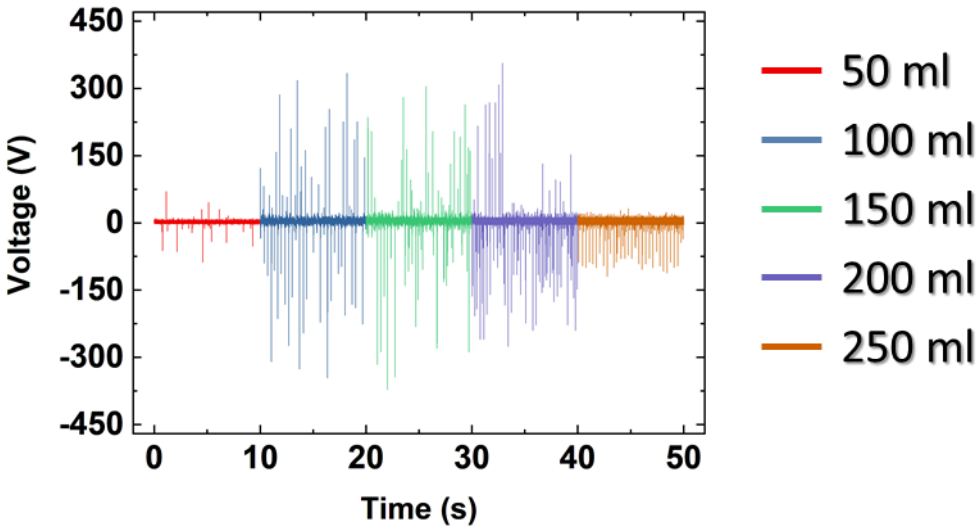

Figure S7. Open-circuit voltage output depending on the total amount of water inside the container. Related to Figure 3.

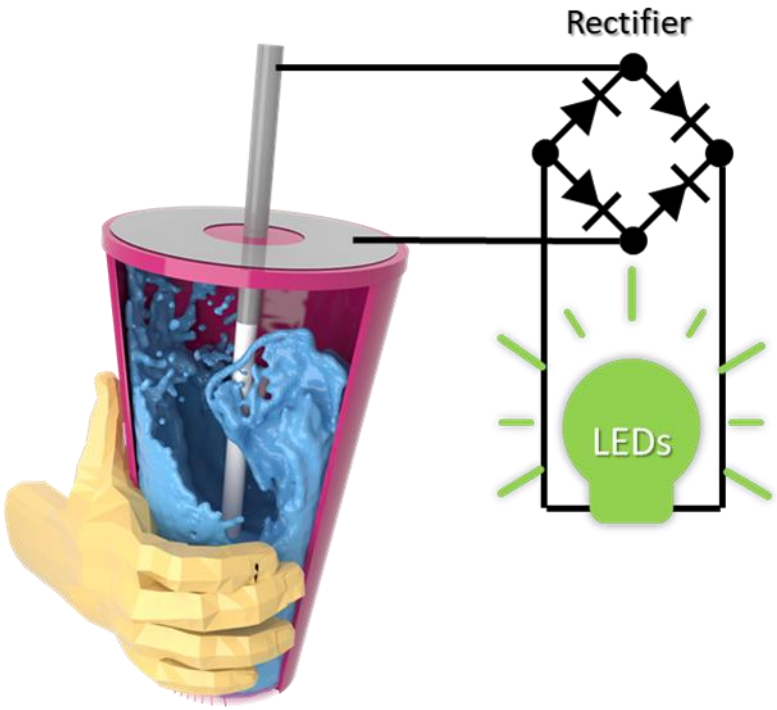

Figure S8. Schematic of rectifier circuit connected to light up LED array. Related to Figure 4.

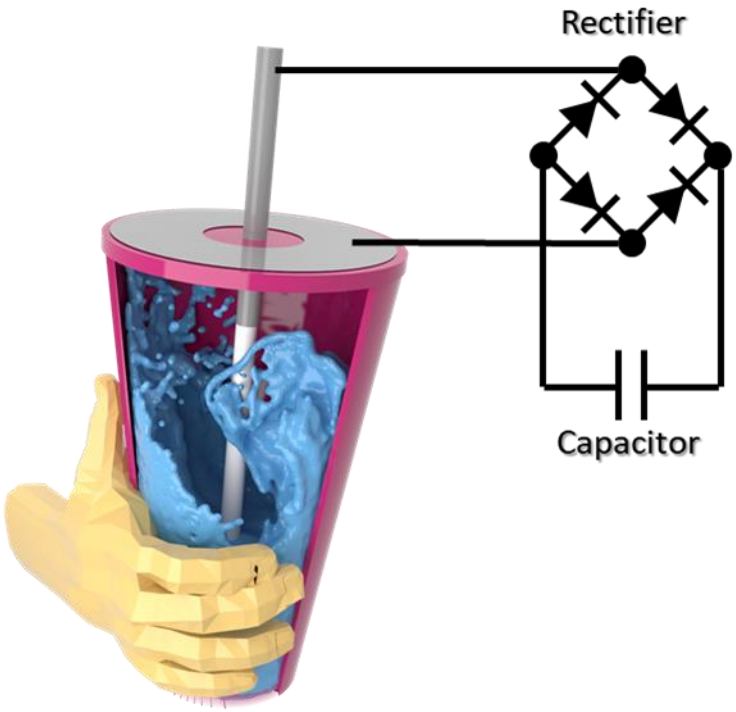

Figure S9. Schematic of rectifier circuit connected to charge commercial capacitor. Related to Figure 4.

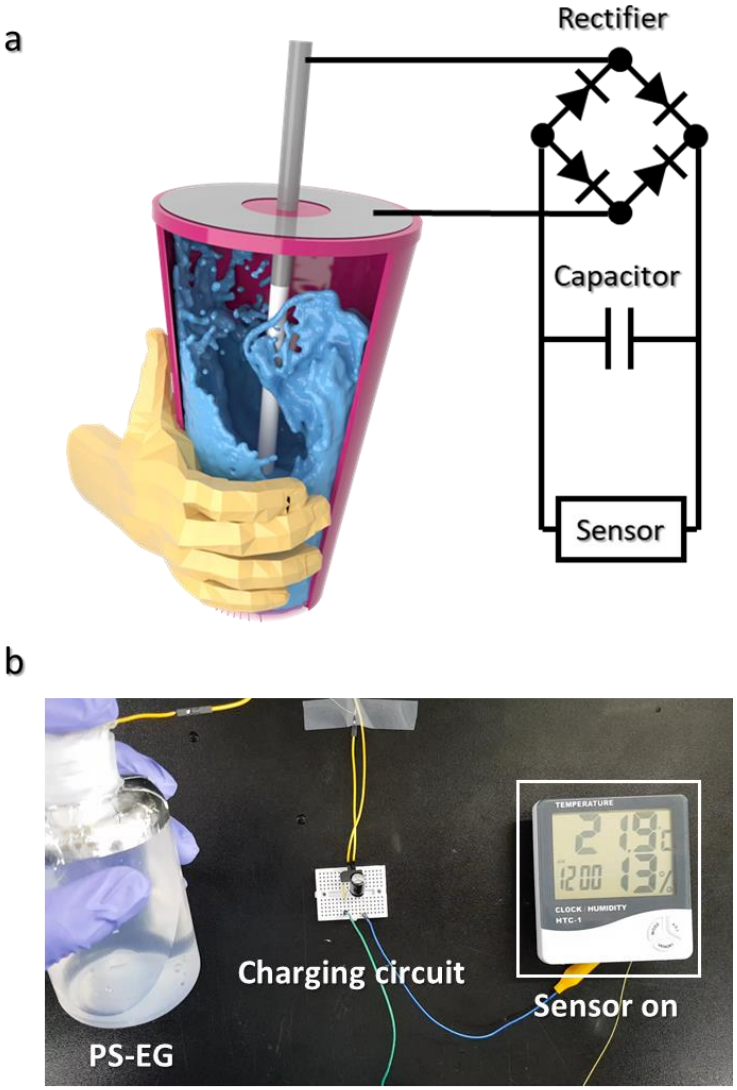

Figure S10. (a-b) Schematic and photograph of charging circuit for powering digital clock temperature-humidity meter. Related to Figure 4.

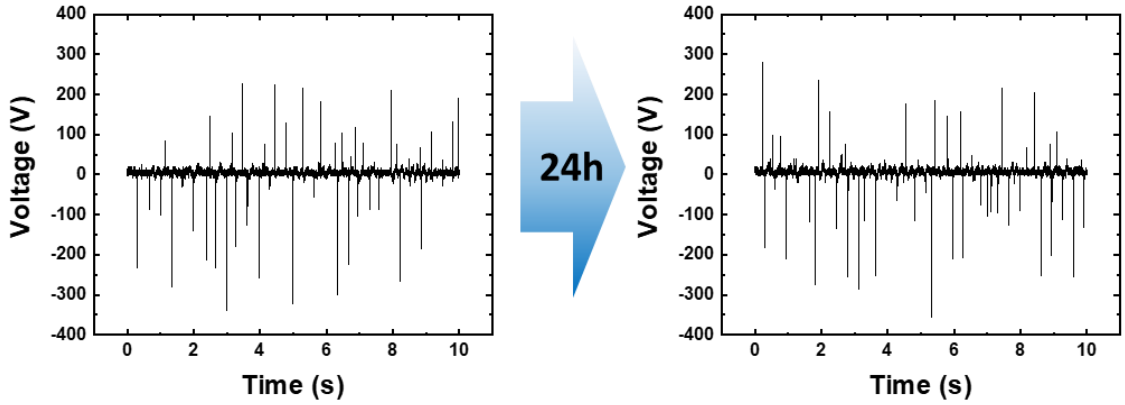

Figure S11. Open-circuit voltage output before and after 24 hours. Related to Figure 4.

Transparent Methods

Fabrication of the PS-EG

A distilled water was utilized throughout this study. A total of 150 mL of distilled water was poured into a 300 mL cylindrical PFA bottle (AS ONE Co.) with a body diameter, body height, neck diameter, and neck height of 6, 10, 2.5, and 2.5 cm, respectively. The neck opening of the PFA bottle was fully sealed using parafilm (PM-996, Bemis Company Inc.) to ensure that the neck was watertight. Subsequently, a polyvinyl chloride (PVC) insulated wire (22 AWG, WISHER Co.) was stripped and inserted through the center of the parafilm and positioned parallel to the wall of the PFA bottle. In particular, a gap of 1 cm was implemented between the water surface and wire end. This wire was used as the central electrode. The neck opening of the PFA bottle was resealed using an insulating adhesive tape. In the h_5 case, an Al tape strip with a length of 2 cm (thickness of 0.05 mm, DUCKSUNG Co.) was attached in a circular manner on the upper side of the PFA bottle, except at the neck, as shown in Figure 2. This Al tape was used as the outer electrode. Furthermore, in the h_1 case, a 4-cm-long Al tape strip was attached in a circular manner at the bottom of the PFA bottle. For the h_2–h_4 cases, a 2-cm-long Al tape strip encircled the body of the PFA bottle at heights of 2.5, 5, and 5 cm, respectively. As shown in Figure 3, a gap of 1 cm was maintained between the water surface and wire, regardless of the water volume.

Experimental setting for the mechanical input

Vertical excitation was provided to the PFA bottle by using a vibration tester (ET-126B-4, Labworks Co.), an amplifier (pa-151, Labworks Co.), and a function generator (AFG3021C, Tektronix Co.). The vibration frequency and amplitude were 6 Hz and 9 mm, respectively.

Electrical measurement

The voltage and current output were measured using an oscilloscope (MDO 3014, Tektronix Co.) and current probe (TCP0030A, Tektronix Co.). To measure the voltage between the central electrode and outer electrode, oscilloscope probes 1 and 2 were connected to the central and outer electrodes, respectively. The voltage output was calculated by subtracting the electric potential of probe 2 from that of probe 1. The current output was measured from the current probe connected directly with the oscilloscope.